Spin blockade in a double quantum dot containing three electrons

S. Amaha,[1,*] W. Izumida,[2] T. Hatano,[3] S. Tarucha,[1,4] K. Kono,[1] and K. Ono[1]

[1]*RIKEN, Center of Emergent Matter Science, 3-1 Wako-shi, Saitama 351-0198, Japan*
[2]*Department of Physics, Tohoku University, Sendai 980-8578, Japan*
[3]*Nuclear Spin Electronics Project, Japan Science and Technology Agency, ERATO, Sendai 980-8578, Japan*
[4]*Department of Applied Physics, School of Engineering, University of Tokyo, 7-3-1 Hongo, Bunkyo-ku, Tokyo 113-8656, Japan*

The realization of a high spin state, which is related to ferromagnetism and molecular magnetism, has been an attractive research topic. Here, using the nonequilibrium condition, we realize a high population of the quadruplet states (total spin $S = 3/2$) in a double quantum dot containing three electrons. Owing to Pauli exclusion, the quadruplet states are forbidden to transit to states with electron double occupancy. Thus, it is located at the end of the dead-end path in a charge transfer cycle, and the three-electron state is stacked at the quadruplet state once it is accessed. As a result of the high population in the three-electron quadruplet spin states, current suppression is observed even under a high bias, which was also reproduced by a simple theoretical model.

PACS number(s): 73.63.Kv, 73.23.Hk

I. INTRODUCTION

Spin effects in molecules and materials are one of the most intriguing topics not only from a scientific viewpoint but also in terms of applications to spintronics and spin-functional devices. In particular, methods of introducing high spin ferromagnetic states in materials associated with magnetization and molecular magnetism have been enthusiastically studied. For example, there are many theoretical approaches to introduce high spin states based on Hubbard models involving the tuning of crystal structures, electron numbers, and band structures [1]. In experiments, molecules with unpaired electrons confined in degenerated levels have been compounded to impart ferromagnetic properties [2]. Most of such theoretical and experimental approaches are based on a spin-dependent exchange interaction (i.e., Hund's coupling), which gives energetic stabilization in spin-paired electrons [3,4].

Here, by carrying out an experimental study on the transport through double quantum dots (DQDs) through a dead-end path in a charge transfer cycle, we investigate a novel method of realizing the highest total spin state [5], which can exhibit ferromagnetic properties. Our weakly coupled DQD contains two QDs (dot L and dot R) with a charge configuration of $(N_L, N_R) = (1, 2)$, where N_L (N_R) is the electron number of dot L (dot R). We observed the characteristic suppression in the charge transfer cycle of $(N_L, N_R) = (0,3) \rightarrow (0,2) \rightarrow (1,2)$. The observed current suppression is attributed to the high population of the highest total spin state in our three-electron DQD (quadruplet state). This is caused by the existence of the dead-end path, as schematically shown in Fig. 1, and the stacking mechanism under a nonequilibrium condition. The fact that current suppression is observed only under a high bias nonequilibrium condition where the dead-end path is accessible in the charge transfer cycle is consistent with our model. Our result demonstrates the feasibility of this method for introducing a ferromagnetic high spin state using Pauli exclusion by a stacking mechanism under a nonequilibrium condition.

---

*Corresponding author: s-amaha@riken.jp

II. EXPERIMENTAL SET UP, MEASUREMENT RESULTS, AND THEORETICAL MODEL

We adopt a vertically coupled DQD formed in a submicron pillar containing a GaAs-Al$_{0.22}$Ga$_{0.78}$As-GaAs triple-barrier structure surrounded by two gate electrodes [6]. Two QDs, dot L and dot R, are formed on the upper and lower wells in the triple-barrier structure, respectively, and the tunnel coupling is sufficiently small [∼0.05 meV (Ref. [7])] for the current to be well described by sequential hopping through the DQD. The difference in the capacitive couplings of the two gate electrodes for two QDs allows us to tune the offset between the two QDs and hence independently manipulate N_L and N_R by applying two different gate voltages V_{g1} and V_{g2} (Ref. [6]). The tunneling current I_d is measured as a function of the source drain voltage V_{sd} and V_{g1} and V_{g2} in a magnetic (B) field applied parallel to I_d at a temperature of ∼0.27 K.

Figure 2(a) shows an intensity plot of I_d in (V_{sd}, V_{g1}) with a constant V_{g2} at zero B field. The charge configurations (N_L, N_R) in Coulomb blockade (CB) regions are assigned by a constant interaction model [8,9]. In Fig. 2(a), the CB regions for $(N_L, N_R) = (0, 1)$ and $(0, 2)$ are open, but the CB region for total electron number $N = 3$ is closed at $V_{g1} = -1.78$ V (lower) and -1.64 V (upper). The energies for the ground states in the three charge configurations, i.e., $(N_L, N_R) = (1, 2)$, $(0, 3)$ and $(0, 2)$ $((N_L, N_R) = (1, 2)$, $(0, 3)$ and $(1, 3))$, are almost degenerate at the lower (upper) closed point of the $N = 3$ Coulomb diamond [10].

The V_{sd}-I_d characteristic is also shown in Fig. 2(b) for $V_{g1} = -1.78$ V and -2 meV $\leqslant V_{sd} \leqslant 5$ meV [from P to Q in Fig. 2(a)]. Here, the suppression I_d clearly occurs for $V_{sd} \sim 1.5 - 3.1$ mV. To clarify the feature around the $N = 3$ CB region in Fig. 2(a), we figure the characteristics in Fig. 2(i). The CB and conducting regions are respectively colored white and pink in Fig. 2(i); the observed I_d-suppressed region, indicated as X, is light blue. A rectangular-conducting island, indicated by the solid red region in Fig. 2(i), is found between region X and the lower right edge of the $N = 3$ CB region. The boundary between region X and the solid red region, denoted as ▲, is observed to be parallel to the lower right edge of the $N = 3$ CB region. Another similar rectangular-conducting
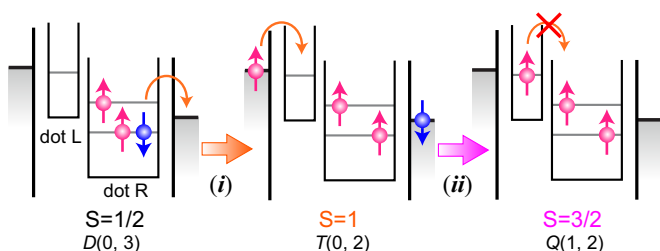
FIG. 1. (Color online) Schematic diagram of stacking process of charge transfer cycle $(0,3) \rightarrow (0,2) \rightarrow (1,2)$ through our DQD. Here, we focus on the condition under which the two levels (ground and excited states) in dot R are accessible. (Left) Schematic of $(0, 3)$ state. Under the high bias condition, transition (i) from the $(0, 3)$ doublet state (total spin $S = 1/2$) to the $(0, 2)$ triplet state ($S = 1$), which is the first excited state in $(0, 2)$, can be realized. The $(0, 2)$ triplet state can be easily accessed because of the exchange energy in dot R. (Middle) Schematic of $(0, 2)$ triplet state. Note that three spin states with $S = 1$ are degenerated at zero magnetic field, but only two up spins are illustrated. By adding one electron, transition (ii) from the $(0, 2)$ triplet state ($S = 1$) to the quadruplet state ($S = 3/2$) can be achieved. (Right) Schematic of $(1, 2)$ quadruplet state. Note that four spin states with $S = 3/2$ are degenerated at zero magnetic field, but three up spins are illustrated. Electron transfer of $(1,2) \rightarrow (0,3)$ is forbidden when the quadruplet state is accessed, resulting in current suppression by the quadruplet spin blockade (Q-SB).

island, indicated by the dashed red hatched region in Fig. 2(i), is also found between region X and the lower right edge of the $N = 4$ CB region. In region X, a faint, almost vertical line associated with the lifting of the current suppression is observed, as shown by $\triangle$ in Fig. 2(i). The measured intensity plots of I_d under constant $B = 0.5$ T, 1.0 T, and 2.0 T are shown in Figs. 2(e)–2(g), respectively. The width of the rectangular island monotonically decreases with increasing B, as plotted in Fig. 2(h).

The observed region X is induced by a spin blockade mechanism, but it has three characteristic differences from the previous observations in the two-electron spin blockade by Pauli exclusion (P-SB) [11]. The first is that the offset energy between the two QDs is different from that in the previous P-SB, so that neither the $(1, 1)$ state nor the $(2n_L +1, 2n_R + 1)$ states (n_L and n_R denote the numbers of single-particle levels in dot L and dot R, respectively) contribute here. Our discussion is limited to the charge state transitions between $(1, 2)$ and $(0, 3)$, and the charge state contributing to the spin blockade is $(1, 2)$. Note that the previously discussed spin blockade mechanisms in a multielectron regime for the $(2n_L + 1, 2n_R + 1)$ states are basically the same as that in $(1, 1)$ P-SB [9,12]. The second difference is in the characteristics of the current-suppressed region. Region X is observed to be away from the edge of the $N = 3$ Coulomb diamond, and two conductive rectangular islands are clearly observed between the edge of the $N = 3$ (or $N = 4$) Coulomb diamond and region X. For the $(1, 1)$ P-SB, the weak current at the boundary between the $(1, 1)$ P-SB and the CB regions was investigated [11], and the characteristic energy scale of the width was almost equal to that of the thermal fluctuation energy (~ 100 μeV). By contrast, the observed energy scale of the width of the islands in Fig. 2(a) is significantly wider than that

in the $(1, 1)$ P-SB. This suggests that a state with significantly large excitation energy contributes to this spin blockade. The third difference is in the arrangement of the two conductive island regions. The electron-hole symmetry was maintained in the $(1, 1)$ P-SB, and the P-SB region was basically symmetric at the center of the $N = 2$ Coulomb diamond [11]. However, the two observed rectangular islands are asymmetric at the center of the $N = 3$ Coulomb diamond, and the electron-hole symmetry should collapse in this spin blockade. The charge transfer cycles relevant to the observed spin blockade are $(1,2) \rightarrow (0,3) \rightarrow (0,2) \rightarrow (1,2)$ for the electron cycle (at the lower closed point of the $N = 3$ Coulomb diamond) and $(1,2) \rightarrow (0,3) \rightarrow (1,3) \rightarrow (1,2)$ (at the upper closed point) for the hole cycle.

The characteristics of region X are also reproduced using the master equation formalism [13]. We solve the rate equations using the transition rate between three quantized levels in the DQD and a constant relaxation rate between only the same spin states. Figure 2(c) shows the calculated I_d obtained by sweeping the energy in dot R (ε_2). The complete reproducibility of region X is confirmed by Figs. 2(a) and (c). The V_{sd}-I_d characteristic at $\varepsilon_2 = -6.6$ meV is also shown in Fig. 2(d).

III. THREE-ELECTRON SPIN BLOCKADE MECHANISM

The charge transfer processes in $(1,2) \rightarrow (0,3) \rightarrow (0,2) \rightarrow (1,2)$ are schematically shown in Fig. 3. At a low V_{sd}, only the ground levels are accessible in the charge transfer cycle, and we cannot expect any spin blockade, as shown in Fig. 3[I]. On the other hand, at a high V_{sd}, the first excited level in dot R becomes accessible, and the electronic spin states in $(1, 2)$ can be classified into two sets of doublet states, $D_1(1, 2)$ (total spin $S = 1/2$ state with triplet state in dot R) and $D_g(1, 2)$ (total spin $S = 1/2$ state with singlet state in dot R), and the quadruplet state $Q(1, 2)$ (total spin $S = 3/2$, see Fig. 3) [14]. If the three-electron highest spin state $Q(1, 2)$ is achieved via the path in Fig. 1 (corresponding to the dead-end path 4→6 in Fig. 3[II]), the charge transfer cycle is stacked at $Q(1, 2)$ with the transition forbidden by Pauli exclusion, resulting in current suppression by the quadruplet state (Q-SB) [15,16]. Note that access to $T(0, 2)$ is necessary to form $Q(1, 2)$. The spin relaxation time from $T(0, 2)$ to $S(0, 2)$ has been measured to be ~ 200 μs [17], which is sufficiently longer than the tunneling time from the source to the DQD (~ 10–100 ns). Then, the $T(0, 2)$ state can be maintained until the next process for $Q(1, 2)$ is achieved. However, the $T(0, 2)$ state is the first excited state containing one electron in the e state; therefore, V_{sd} must be increased to access the $T(0, 2)$ state with the excitation energy from the ground state [$S(0, 2)$, see Fig. 3]. Thus, region X is observed not close to but away from the $N = 3$ CB region. The width of the rectangular conductive islands in the electron (hole) cycle corresponds to the excitation energy from the ground state of the $N = 2$ ($N = 4$) singlet to the $N = 2$ ($N = 4$) triplet excited state. Basically, their excitation energies are simply expected to equal the energy difference between the g and e levels in dot R. Moreover, as B increases, the two boundaries of regions X, ▲, and ■ are expected to approach the boundary of the CB region due to the stabilization of the e level from the diamagnetic shift in the single-particle
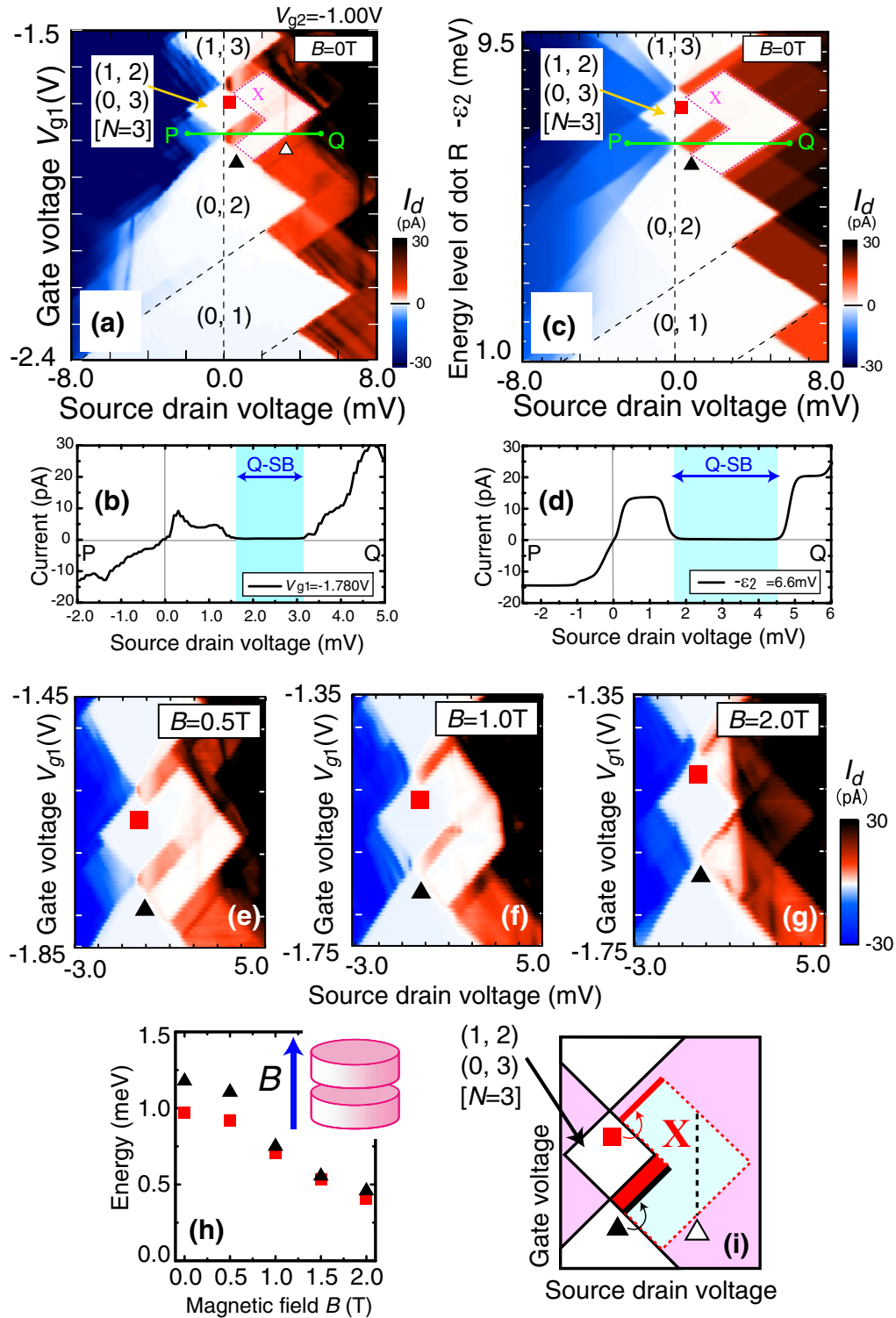
FIG. 2. (Color online) (a) Measured I_d at $V_{g2} = -1.0$ V plotted in (V_{sd}, V_{g1}) at $B = 0$ T. (b) Cross section of the observed I_d plot along the green line in (a). (c) I_d calculated by the master equation approach. (d) Cross section of calculated I_d along the green line in (c). Measured I_d at $V_{g2} = -1.05$ to -1.12 V in (V_{sd}, V_{g1}) at $B = $ (e) 0.5 T, (f) 1.0 T, and (g) 2.0 T. (h) B-field evolution of the width of islands located between ▲ (■) and the boundary of the $N = 3$ ($N = 4$) CB region, corresponding to the excitation energy from the ground state to the first excited $T(0, 2)$ state. (i) Magnified diagram around $N = 3$ Coulomb diamond in (a).

level [4]. The observed B-field evolutions of the separation between ▲ (■) and the edge of the $N = 3$ CB region are also shown in Fig. 2(h). They decrease toward zero with increasing B, in accordance with our expectation [4]. The vertical dark

region of higher V_{sd} in Figs. 2(e)–2(g), with a current threshold running parallel to the vertical axis (V_{g1}), is caused by access to the $Q(0, 3)$ state, for which one electron in the third excited level of dot R is allowed to be occupied.

IV. GENERALIZED SPIN BLOCKADE MECHANISM

So far, we have described the experimental observation of a three-electron spin blockade in a DQD. However, this spin blockade mechanism itself is not specific to our three-electron and three-site system; it can also be generalized to multielectron and multisite systems. To identify the essence of the current suppression mechanism, we discuss in detail the simplified charge/spin state transition diagram shown in Fig. 3. In Fig. 3[II], we present all the dominant electronic states contributing to the spin blockade with indices $i = 1$–6. The arrows in Fig. 3[II] indicate the transitions between two contributing states, and the rates from the j state to the i state are denoted by γ_{ij} ($i, j = 1$–6). Owing to the finite-bias

condition, we neglect the electron transfer processes with energy absorption; therefore, the transitions in Fig. 3 are presented by unidirectional rather than bidirectional arrows.

In $Q(1, 2)$, electrons are forbidden to transit to other states owing to Pauli exclusion. Therefore, the transition rates from $Q(1, 2)$ satisfy the following relation [18]:

$$\forall i \in \{1,2,3,4,5\}; \gamma_{i6} = 0 \text{ and } \exists i \in \{1,2,3,4,5\}; \gamma_{6i} \neq 0,$$

where we assume that it is forbidden to transit from $Q(1, 2)$ to elsewhere via co-tunneling processes. Here, to estimate the population of each state, the rate equation for the probabilities of the contributing states [p_i, $i = 1$–6 in Fig. 3[II]] in the steady state is expressed as

$$\frac{d}{dt}\begin{pmatrix} p_1 \\ p_2 \\ p_3 \\ p_4 \\ p_5 \\ p_6 \end{pmatrix} = \begin{pmatrix} -\gamma_{21}-\gamma_{41} & 0 & \gamma_{13} & 0 & \gamma_{15} & 0 \\ \gamma_{21} & -\gamma_{32} & 0 & 0 & 0 & 0 \\ 0 & \gamma_{32} & -\gamma_{13} & 0 & 0 & 0 \\ \gamma_{41} & 0 & 0 & -(\gamma_{54}+\gamma_{64}) & 0 & 0 \\ 0 & 0 & 0 & \gamma_{54} & -\gamma_{15} & 0 \\ 0 & 0 & 0 & \gamma_{64} & 0 & 0 \end{pmatrix}\begin{pmatrix} p_1 \\ p_2 \\ p_3 \\ p_4 \\ p_5 \\ p_6 \end{pmatrix} = 0.$$

Note that $\sum_i^6 p_i = 1$ and that we consider the sequential tunneling processes. From this, we obtain the following solution:

$$(p_1,p_2,p_3,p_4,p_5,p_6) = (0,0,0,0,0,1).$$

This means that the state is stacked at $Q(1, 2)$. Note that p_1, p_2, and p_3 become finite according to the rate equation under the low-bias condition [Fig. 3[I]]. The key to producing the stacking at $Q(1, 2)$ is the existence of the dead-end path. The stacking state $Q(1, 2)$ is located at the end of the dead-end path, and there is no outgoing rate from this stacking state [18]. Coincidentally, it is possible to reach 6 ($Q(1,2)$) from all other states in a finite number of steps by following the arrows in Fig. 3[II]. Therefore, the state eventually becomes stacked at 6 sooner or later [18]. Even in multiply coupled QDs, this mechanism becomes effective if the transition diagram can be designed to have a dead-end path. In particular, the electrons in the highest spin state cannot transit to other states with double occupancy owing to Pauli exclusion; therefore, it is easy to design the highest spin state to be at the end of dead-end path when the co-tunneling processes to escape from the highest spin state are neglected [15]. As many types of CB-dominated blocking mechanism [19,20] have been demonstrated, our Pauli exclusion-dominated blocking mechanism can generally be found in more complex systems with spin effects.

Note that not only the design of the dead-end path but also nonequilibrium is important in this mechanism. How the dead-end path works has already been discussed in detail, so here we make two comments on the effect of the nonequilibrium condition. The first is that the state transitions in Fig. 3 are indicated by unidirectional rather than bidirectional arrows owing to the nonequilibrium condition. The second is that a power supply is required to stack the system in the highest spin state. This is because an energy supply is required to transfer electrons from the source electrode to

the drain electrode until the dead-end path is accessed and the charge transfer cycle is stacked. A simple evaluation of this required energy suggests that higher energies are required as the number of electrons increases. Therefore, we can expect that the observation of a spin blockade in coupled QDs may become more difficult as the number of electrons increases.

Finally, we discuss how our spin blockade mechanism contributes to the realization of ferromagnetic states in coupled QDs. The three-electron spin state, which is realized in this experiment, is a mixed state consisting of four different S_z states ($S_z = +3/2, +1/2, -1/2,$ and $-3/2$) with maximum total spin $S = 3/2$. To obtain ferromagnetic properties, a purification process to select the state with the component having highest spin for one direction, i.e., $S_z = +3/2$ is required. A possible process is simply to apply an external B field so that the lowest energy state in the quadruplet ($S_z = +3/2$) is favored by Zeeman energy splitting. However, adjustments of the external B field and source drain voltage are required to realize high population of the lowest energy state in quadruplet: (1) Zeeman splitting is sufficiently larger than the thermal energy and (2) the source drain voltage is adjusted so that the lowest energy state in quadruplet is accessible.

V. CONCLUSION

We investigate the spin blockade of three-electron spin in a DQD. Here, the three-electron state is stacked at the highest total spin state (quadruplet) via the dead-end path in the charge transfer cycle. Under this stacking condition, the highest total spin state of the three electrons is highly populated in a three-electron DQD as a result of Pauli exclusion. This method can be mathematically generalized [14] and is applicable not only to three-electron DQD but also to multiply coupled QD systems, molecules, and materials. Our results
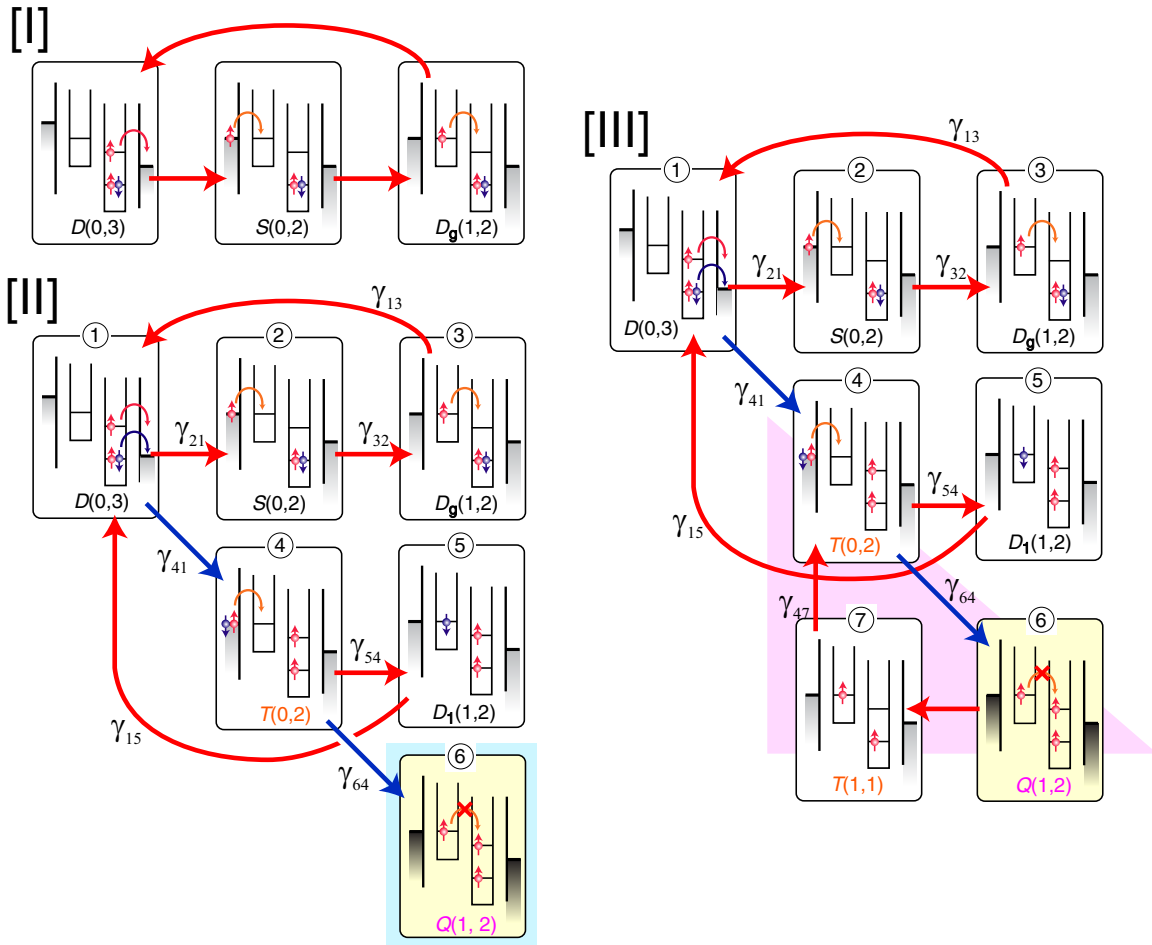
FIG. 3. (Color online) Schematics of charge and spin states and their transitions in $(0,3) \rightarrow (0,2) \rightarrow (1,2) \rightarrow (0,3)$ in [I] low, [II] medium (Q-SB), and [III] high V_{sd} regions in Figs. 2(a) and (c). The total spin of each state is shown by the indices S (total spin $S = 0$), $D(S = 1/2)$, $T(S = 1)$, and $Q(S = 3/2)$. $D_g(1, 2)$ is the ground state of the $(1, 2)$ charge state, and $D_1(1, 2)$ is explained in the text. Here, we present the first-order tunneling processes through outer and inner tunneling barriers by arrows. Transitions from $D(0, 3)$ to $T(0, 2)$ and from $T(0, 2)$ to $Q(1, 2)$ in [II] correspond to the region where the dead-end path in Fig. 1 is accessible and the Q-SB is observed in Figs. 2(a) and 2(c). In the high V_{sd} region, the spin blockade is lifted because the dead-end path is released through $6 \rightarrow 7 \rightarrow 4$, as shown in [III] (highlighted in red).

highlight the intriguing physics that occur under nonequilibrium conditions and provide a novel tool for introducing the highest total spin state, which may exhibit ferromagnetic properties in various materials. This will be verified in future experiments.

APPENDIX A: ASSIGNMENT OF CHARGE STATES IN HONEYCOMB DIAGRAM AND COULOMB DIAMONDS USING A CONSTANT INTERACTION (CI) MODEL

In the main text, we omitted the details of the device structure and the technique used to assign the charge states. The DQD we studied is formed in a submicron circular mesa structure containing a GaAs-Al$_{0.22}$Ga$_{0.78}$As-GaAs triple-barrier structure surrounded by two Schottky gate electrodes. Figure 4(a) shows a schematic diagram of our device structure, which is basically similar to our previously studied vertical DQD device with a 60 Å center barrier. The fabrication process is discussed in Ref. [21]. The two gate voltages allow us to modify the offset between the two QDs as a function of (V_{g1}, V_{g2}) [6]. The charge state (N_L, N_R) can be assigned using the well-studied CI model [8,9]. From the two observed kinks denoted by ● in Fig. 4(d), we find that zero (two) electrons are trapped in dot L (dot R), i.e., (N_L, N_R) = (0, 2) slightly on the negative side of the yellow square. The characteristic positions (▲ and ●) in the Coulomb diamonds in Fig. 4(d) can also be reproduced by the CI model [6,8,9]. Thus, the
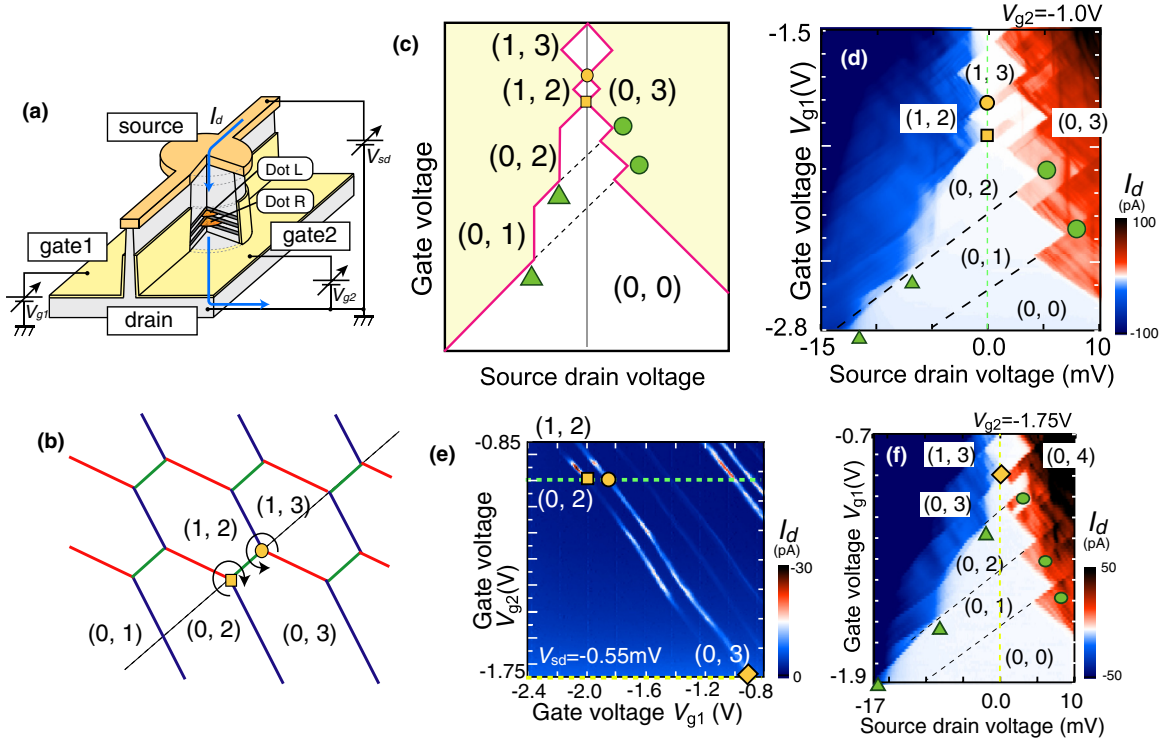
FIG. 4. (Color online) (a) Schematic diagram of two-gate vertical DQD device. (b) Charge stability diagram of DQD. The sweeping direction of V_{g2} can be approximately assigned to that of the dotted line in (b). (c) Coulomb diamond obtained using the CI model for the DQD. Two kinks (green circles) and vertical lines (green triangles) are observed, and the charge states of Coulomb blockade regions are also shown. (d) Coulomb diamonds for conditions of Fig. 2(a) [$V_{g2} = -1.0$ V, green dotted line in (e)] plotted with a relatively large scale. (e) Coulomb oscillation lines as a function of (V_{g1}, V_{g2}). The characteristic points are also shown as a yellow diamond, square, and circle in (d) to (f). (f) Coulomb diamonds obtained by sweeping V_{g1} at $V_{g2} = -1.75$ V [yellow dotted line in (e)]. Three pairs of kinks (green circles) and vertical lines (green triangles) are identified; therefore, the charge state slightly below the closed Coulomb diamond (yellow diamond) is assigned to (0, 3), implying that the offset energy between the two QDs can be modulated by adjusting V_{g2}.

charge transfer cycles at positive V_{sd} near the closed Coulomb diamond, as shown by □ and ○, are assigned to (N_L, N_R) = (0,2) → (1,2) → (0,3) → (0,2) [process α] and (1,3) → (1,2) → (0,3) → (1,3) [process β], respectively. Figure 4(e) shows the observed Coulomb oscillation lines as a function of (V_{g1}, V_{g2}). Because the cross-capacitance is relatively small and the two gates are nominally equally coupled [6], the Coulomb oscillation lines are observed to be almost parallel, and the offset between the two QDs can be roughly modified by changing the scanning position (V_{g1}, V_{g2}) by changing the value of V_{g2}. Figure 4(f) shows Coulomb diamonds obtained by sweeping V_{g1} at $V_{g2} = -1.75$ V. Three pairs of kinks and vertical lines are observed in Fig. 4(f), suggesting that the offset between the two QDs can be modulated by adjusting V_{g2}.

APPENDIX B: ELECTRONIC STATE TRANSITIONS IN HOLE CYCLE OF (1, 2) QUADRUPLET SPIN BLOCKADE

In the main text, we described the charge state transitions in the electron states for the (1, 2) Q-SB. However, we also found clear current suppression in the so-called hole cycle (0,3) → (1,3) → (1,2) → (0,3). Here, we focus on this cycle to explain how the boundary of region X is defined, as shown in Fig. 5. By injecting one electron, the initial doublet state $D(0, 3)$ can transit to the singlet state $S(1, 3)$ or the triplet state $T(1, 3)$.

The energy difference between $S(1, 3)$ and $T(1, 3)$ has been estimated to be $\sim$10 μeV (Ref. [22]). At a low bias, both $S(1, 3)$ and $T(1, 3)$ are only allowed to transit to $D_g(1, 2)$. However, at a high bias ($V_{sd} > \Delta E_{Q-Dg}$, ΔE_{Q-Dg} is the energy difference between $D_g(1, 2)$ and $Q(1, 2)$), $T(1, 3)$ can undergo a transition to $Q(1, 2)$, resulting in the current being blockaded, indicated as [hl] in Fig. 5(b). Note that ΔE_{Q-Dg} also roughly equals 2 meV, that is, ΔE_{S-T} minus the exchange energy between $T(1, 3)$ and $S(1, 3)$. Note that the energy separation between $T(1, 3)$ and $S(1, 3)$ is about $\sim$0.1 mV (Ref. [22]) and that the spin relaxation from $T(1, 3)$ to $S(1, 3)$ is typically measured to be $\sim$10^4–10^5 μs [12], which is considerably longer than the tunneling time for the drain Γ_R ($\sim$10–100 ns) [23]. Moreover, $T(1, 3)$ remains in a relaxed state until the loading process of $Q(1, 3)$. Note that the asymmetry in the electron and hole cycles in the Q-SB is introduced by the difference between the preparation processes of the triplet state in Figs. 5(a) and 5(b).

APPENDIX C: DETAILS AND PARAMETERS OF THE THEORETICAL APPROACH TO QUADRUPLET SPIN BLOCAKDE

To examine the Q-SB region X theoretically, we performed a calculation using the master equation [13,15]. The Hamiltonian used to describe the electronic states in the DQD
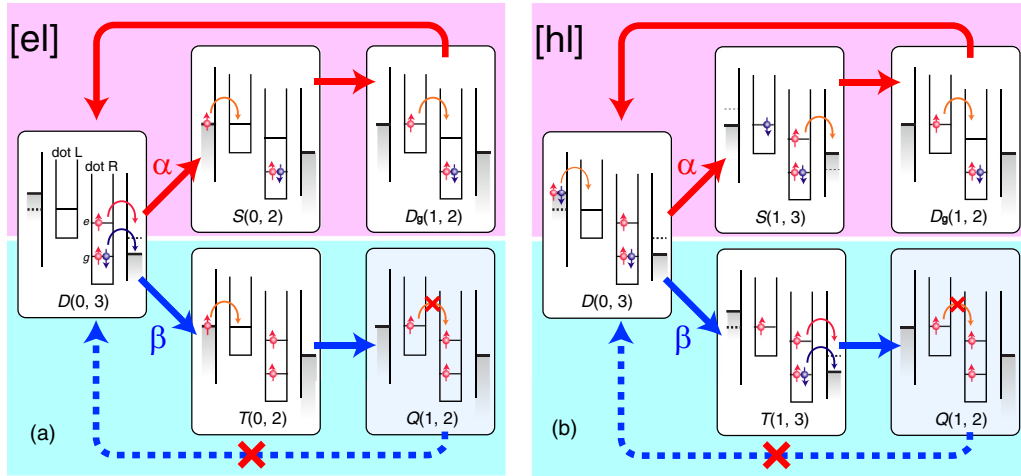
FIG. 5. (Color online) Charge transfer cycles for (a) electron and (b) hole with consideration of the spin effect.

can be presented as

$$H_d = \sum_{i=1,\sigma=\uparrow,\downarrow}^{3} \varepsilon_{i,\sigma} n_{i,\sigma} + \sum_{i=1}^{3} U_i n_{i,\uparrow} n_{i,\downarrow} + V_{12} n_1 n_2 + V_{23} n_2 n_3$$
$$+ V_{31} n_3 n_1 + \sum_{i,j} J_{ij} \vec{S}_i \cdot \vec{S}_j$$
$$+ \sum (t_{12} a_{1,\sigma}^{\dagger} a_{2,\sigma} + t_{31}^* a_{1,\sigma}^{\dagger} a_{3,\sigma} + \text{H.c.}).$$

Here, we consider a single level ($i = 1$) in dot L and two levels (a lower level of $i = 2$ and a higher level of $i = 3$) in dot R. Also, $\varepsilon_{i,\sigma}$ ($i = 1, 2, 3$) are the single-particle energies of each level, U_i ($i = 1, 2, 3$) are the intralevel Coulomb energies, V_{ij} ($i = 1, 2, 3, i \neq j$) are the interlevel Coulomb energies, J_{ij} are the

exchange energies between two levels, and t_{ij} ($i, j = 1, 2, 3, i \neq j$) are the tunnel coupling energies between levels. Here, we diagonalize the Hamiltonian H_d, solve the rate equations using the estimated transition probability of each level for the source and drain electrodes, and statistically evaluate the tunneling current through the DQD. Note that we have not considered any spin-mixing effects (such as spin orbit and hyperfine coupling) in the calculations presented here. The parameters we adopted for our calculation are $\varepsilon_1 = \Delta + 2 (V_{23} - V_{12})$, $\varepsilon_3 = \varepsilon_2 + \Delta$ [$\Delta = 0.22U$: the energy difference between the $1s$ (ground) and $2p$ (first excited) levels in dot R], $U_1 = U_2 = U = 3.0$ meV, $U_3 = 1.3U = 3.9$ meV, $V_{12} = 0.55U$, $V_{23} = U$, $V_{31} = 0.45U$, $J_{12} = 0$, $J_{23} = -0.05U$, $J_{31} = 0$, $t_{12} = 0.05U$, and $t_{31} = 0.01U$. Note that the difference between t_{12} and t_{31} is associated with the difference between the angular momentum of the contributing states [22] and that J_{23} corresponds to the exchange energy in dot R, which stabilizes the triplet state (Hund's coupling energy [4]). The coupling strengths between
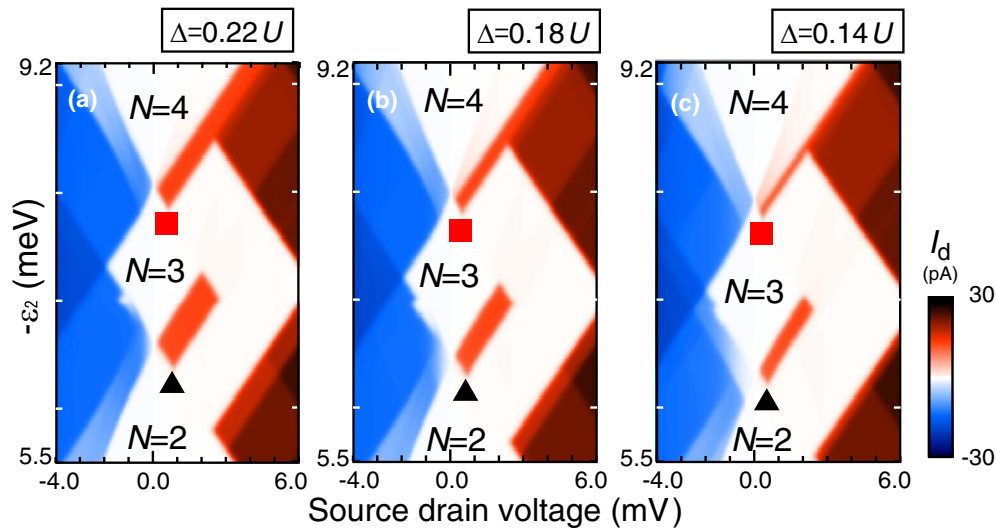
FIG. 6. (Color online) Calculated Coulomb diamonds as a function of the single-particle energy separation Δ between the ground ($1s$) and excited ($2p$) states. The separation Δ is set to (a) $0.22U$, (b) $0.18U$, and (c) $0.14U$.

the source and drain electrodes are $\Gamma_s = \Gamma_d = 0.15 \times 10^{-4} U$. The strength of both the intradot and interdot energy relaxation γ is assumed to be $\gamma = 10^{-3} U$, and the temperature T in the calculation is 300 mK. The single-particle levels in dot L and dot R are assumed to be linearly modulated for the source drain voltage V_{sd} [6,8,15].

APPENDIX D: DEPENDENCE OF THE SPIN BLOCKADE REGION ON SINGLET TRIPLET ENERGY OBTAINED BY THEORETICAL APPROACH

In Figs. 2(e)–2(h) of the main text, we showed the B-field dependence of the boundary of region X (the Q-SB region). The same dependence is also reproduced by the theoretical calculation discussed in Appendix C. The confinement potential for electrons in a QD can be roughly described as a two-dimensional harmonic potential with anisotropy [24], and the second level ($2p$ state in atomlike notation)

is expected to be stabilized by the B field originating from the diamagnetic shift in the Fock-Darwin spectrum. Figure 6 shows the theoretically obtained Coulomb diamonds as a function of the energy separation Δ between the first ($1s$) and second ($2p$) energy levels. The boundaries indicated by ■ and ▲ are the shifted boundaries of the $N = 4$ and $N = 3$ CB regions, respectively, and the results are in good agreement with the behavior shown in Figs. 2(e)–2(g).

APPENDIX E: MARKOV CHAINS OF CHARGE TRANSFER CYCLE IN SPIN BLOCKADE REGIME

In the main text, by considering the rate equations we discussed the transfer cycle, statistically estimated the population of each state, and referred to the path toward the stacking state as the dead-end path. Here, we discretize the time as $t = n\Delta T$ (n is the integer and ΔT is the unit of time) and express the rate equations as

$$
\begin{pmatrix} p_1^{n+1} \\ p_2^{n+1} \\ p_3^{n+1} \\ p_4^{n+1} \\ p_5^{n+1} \\ p_6^{n+1} \end{pmatrix} = \begin{pmatrix} 1 + (-\gamma_{21} - \gamma_{41})\Delta t & 0 & \gamma_{13}\Delta t & 0 & \gamma_{15}\Delta t & 0 \\ \gamma_{21}\Delta t & 1 - \gamma_{32}\Delta t & 0 & 0 & 0 & 0 \\ 0 & \gamma_{32}\Delta t & 1 - \gamma_{13}\Delta t & 0 & 0 & 0 \\ \gamma_{41}\Delta t & 0 & 0 & 1 - (\gamma_{54} + \gamma_{64})\Delta t & 0 & 0 \\ 0 & 0 & 0 & \gamma_{54}\Delta t & 1 - \gamma_{15}\Delta t & 0 \\ 0 & 0 & 0 & \gamma_{64}\Delta t & 0 & 1 \end{pmatrix} \begin{pmatrix} p_1^n \\ p_2^n \\ p_3^n \\ p_4^n \\ p_5^n \\ p_6^n \end{pmatrix}
$$

$$
= \begin{pmatrix} 1 + (-\Gamma_{21} - \Gamma_{41}) & 0 & \Gamma_{13} & 0 & \Gamma_{15} & 0 \\ \Gamma_{21} & 1 - \Gamma_{32} & 0 & 0 & 0 & 0 \\ 0 & \Gamma_{32} & 1 - \Gamma_{13} & 0 & 0 & 0 \\ \Gamma_{41} & 0 & 0 & 1 - (\Gamma_{54} + \Gamma_{64}) & 0 & 0 \\ 0 & 0 & 0 & \Gamma_{54} & 1 - \Gamma_{15} & 0 \\ 0 & 0 & 0 & \Gamma_{64} & 0 & 1 \end{pmatrix} \begin{pmatrix} p_1^n \\ p_2^n \\ p_3^n \\ p_4^n \\ p_5^n \\ p_6^n \end{pmatrix}
$$

$$
\equiv \begin{pmatrix} Q & 0 \\ {}^t R & 1 \end{pmatrix} \vec{p}^n = P \vec{p}^n.
$$

Here, we define $\Gamma_{ij} = \gamma_{ij}\Delta t$ ($i, j = 1$–6). This means that the charge transfer cycle in Fig. 3[II] can be regarded as a Markov

chain with the transition matrix P. The transition diagram of this Markov chain is presented in Fig. 7.

Using Fig. 7, we can easily identify the Markov chain in Fig. 3[II] as one of the absorbing Markov chains: the six state in Fig. 3[II] is the absorbing state, and it is possible to reach the six state (absorbing state) from the other five states in a finite number of steps [25].

APPENDIX F: EVALUATION OF ENERGY IN ACCESS PROCESS TO HIGH SPIN STATE

Under the thermal equilibrium condition, we expect that there will be no flows of energy. In electron transport, electrons usually carry the energy. In a spin-blockaded DQD, there are no currents through the DQD; therefore, no flows of energy are expected. Thus, it appears that the spin blockade can be realized under the equilibrium condition. However, we

FIG. 7. Transition diagram of Markov chain in Fig. 3[II].

emphasized that the nonequilibrium condition is important for our spin blockade mechanism. Here, we explain how the energy flow, which requires a nonequilibrium condition, can be found in our spin blockade mechanism.

The main energy supplied in the nonequilibrium condition is the work carried out to transfer electrons from the source electrode to the drain electrode until the dead-end path is accessed. By considering the Markov process, we can simply and roughly obtain the work carried out to access the spin-blockaded states in (i) a two-electron DQD (P-SB), (ii) a three-electron DQD (Q-SB), and (iii) a multiple N-electron coupled QD.

(i) Two-electron DQD: In the electron-injection process, one state is selected from three triplet states and one single state. The probability that the triplet is accessed is $\sim 3/4$. The work carried out to realize the P-SB in the first injection process and its probability are 0 and $\sim 3/4$, respectively. Those in the second injection process are w and $\sim 1/4 \times 3/4$, respectively. Here, we assume that the work carried out to transfer a single electron from the source electrode to the drain electrode is roughly constant as $\sim w$. Those in the third injection process are $w + w$ and $\sim 1/4 \times 1/4 \times 3/4$, respectively. Thus, we can estimate the amount of work as

$$W \sim \frac{3}{4} \sum_{i=1}^{\infty} \left(\frac{1}{4}\right)^i \times i \times w = \frac{3w}{4} \sum_{i=1}^{\infty} \frac{i}{4^i}$$

$$= \frac{3w}{4} \frac{1/4}{(1 - 1/4)^2} = \frac{w}{3}.$$

(ii) Three-electron DQD: In the electron-injection process, one state is selected from four quadruplet and four doublet states. The probability that the quadruplet is accessed is $\sim 1/2$. Thus, we can estimate the amount of work as

$$W \sim \frac{1}{2} \sum_{i=1}^{\infty} \left(\frac{1}{2}\right)^i \times i \times w = \frac{w}{2} \sum_{i=1}^{\infty} \frac{i}{2^i} = \frac{w}{2} \frac{1/2}{(1 - 1/2)^2} = w.$$

(iii) N-electron coupled QD: In the electron-injection process, the total number of states and the number of highest spin states are 2^N and $N + 1$, respectively. Thus, the probability p that the highest spin state is accessed is $p \sim (N + 1)/2^N$ (we use $q = 1 - p$ in the following notation). Thus, we can estimate the amount of work as

$$W = p \sum_{i=1}^{\infty} q^i \times i \times w = pw \sum_{i=1}^{\infty} i q^i = pw \frac{q}{(1 - q)^2}$$

$$= \frac{qw}{1 - q} = \frac{(1 - p)w}{p}.$$

For a sufficiently large N, $p \ll 1$. Therefore, the expected amount of work is

$$W = \frac{(1 - p)w}{p} \sim \frac{w}{p} = \left(\frac{2^N}{N}\right) w.$$

If the number of electrons increases, the amount of work carried out until the spin-blockaded highest spin state is accessed is expected to exponentially increase.

[1] A. Mielke and H. Tasaki, Commun. Math. Phys. **158**, 341 (1993).

[2] M. Kinoshita, P. Turek, M. Tamura, K. Nozawa, D. Shiomi, Y. Nakazawa, M. Ishikawa, M. Takahashi, K. Awaga, T. Inabe, and Y. Maruyama, Chem. Lett. **20**, 1225 (1991).

[3] M. Korkusinski, I. P. Gimenez, P. Hawrylak, L. Gaudreau, S. A. Studenikin, and A. S. Sachrajda, Phys. Rev. B **75**, 115301 (2007).

[4] L. P. Kouwenhoven, T. H. Oosterkamp, M. W. S. Danoesastro, M. Eto, D. G. Austing, T. Honda, and S. Tarucha, Science **278**, 1788 (1997).

[5] Here we realize the mixed state of the highest total spin states in three-electron spin ($S_z = +3/2, +1/2, -1/2, -3/2$). A process to purify the direction of electron spin is described later.

[6] R. Takahashi, K. Kono, S. Tarucha, and K. Ono, Phys. Rev. Lett. **107**, 026602 (2011).

[7] S. Amaha, D. G. Austing, Y. Tokura, K. Muraki, K. Ono, and S. Tarucha, Solid State Commun. **119**, 183 (2001); M. Rontani, S. Amaha, K. Muraki, F. Manghi, E. Molinari, S. Tarucha, and D. G. Austing, Phys. Rev. B **69**, 085327 (2004).

[8] T. Ota, K. Ono, M. Stopa, T. Hatano, S. Tarucha, H. Z. Song, Y. Nakata, T. Miyazawa, T. Ohshima, and N. Yokoyama, Phys. Rev. Lett. **93**, 066801 (2004); A. Fuhrer, L. E. Fröberg, J. N. Pedersen, M. W. Larssen, A. Wacker, M.-E. Pistol, and L. Samuelson, Nano Lett. **7**, 243 (2007).

[9] S. Amaha, T. Kodera, T. Hatano, K. Ono, Y. Tokura, S. Tarucha, J. A. Gupta, and D. G. Austing, J. Phys. Soc. Jpn. **80**, 023701 (2011).

[10] The energies of these three charge configurations are adjusted within the tunnel coupling energy (~ 0.05 meV) between two QDs.

[11] K. Ono, D. G. Austing, Y. Tokura, and S. Tarucha, Science **297**, 1313 (2002).

[12] A. C. Johnson, J. R. Petta, C. M. Marcus, M. P. Hanson, and A. C. Gossard, Phys. Rev. B **72**, 165308 (2005).

[13] J. Fransson and M. Råsander, Phys. Rev. B **73**, 205333 (2006).

[14] E. A. Laird, J. M. Taylor, D. P. DiVincenzo, C. M. Marcus, M. P. Hanson, and A. C. Gossard, Phys. Rev. B **82**, 075403 (2010); L. Gaudreau, G. Granger, A. Kam, G. C. Aers, S. A. Studenikin, P. Zawadzki, M. Pioro-Ladrière, Z. R. Wasilewski, and A. S. Sachrajda, Nat. Phys. **8**, 54 (2012); S. Amaha, T. Hatano, H. Tamura, S. Teraoka, T. Kubo, Y. Tokura, D. G. Austing, and S. Tarucha, Phys. Rev. B **85**, 081301(R) (2012); T. Hatano, Y. Tokura, S. Amaha, T. Kubo, S. Teraoka, and S. Tarucha, *ibid.* **87**, 241414(R) (2013).

[15] S. Amaha, W. Izumida, T. Hatano, S. Teraoka, S. Tarucha, J. A. Gupta, D. G. Austing, Phys. Rev. Lett. **110**, 016803 (2013).

[16] In contrast to that in the previous work, the Q-SB is completely assigned in Figs. 2(a) and (c). Two points with significant novelty are achieved: (i) the realization of spin polarization with no external B field but through a self-polarizationlike process, and (ii) the reproducibility of the observed Q-SB by a simple theoretical model.

[17] T. Fujisawa, D. G. Austing, Y. Tokura, Y. Hirayama, and S. Tarucha, Nature **419**, 278 (2002); A. C. Johnson, J. R. Petta, J. M. Taylor, A. Yacoby, M. D. Lukin, C. M. Marcus, M. P. Hanson, and A. C. Gossard, *ibid.* **435**, 925 (2005).

[18] By discretizing the steps of time, the charge/state transfer processes in Fig. 3 are regarded as Markov processes, and the stacking state and the charge/state transfer cycle in Fig. 3[II] correspond to an absorbing state and an absorbing Markov chain, respectively.

[19] M. Stopa, Phys. Rev. Lett. **88**, 146802 (2002).

[20] G. A. Cecchi and M. O. Magnasco, Phys. Rev. Lett. **76**, 1968 (1996).

[21] D. G. Austing, T. Honda, and S. Tarucha, Jpn. J. Appl. Phys. **34**, 1320 (1995).

[22] T. Kodera, K. Ono, Y. Kitamura, Y. Tokura, Y. Arakawa, and S. Tarucha, Phys. Rev. Lett. **102**, 146802 (2009).

[23] T. Fujisawa, D. G. Austing, Y. Tokura, Y. Hirayama, and S. Tarucha, Phys. Rev. Lett. **88**, 236802 (2002).

[24] Y. Tokura, S. Sasaki, D. G. Austing, and S. Tarucha, Physica B **298**, 260 (2001).

[25] C. M. Grinstead and J. L. Snell, *Introduction of Probability* (American Mathematical Society, Providence, RI, 1997), Chap. 11.